Environ Geol (2007) 52:1277–1296
DOI 10.1007/s00254-006-0567-8

ORIGINAL ARTICLE

Mineralogical and geochemical constraints on environmental impacts from waste rock at Taojiang Mn-ore deposit, central Hunan, China

Bo Peng · Adam Piestrzynski · Jadwiga Pieczonka · Meilian Xiao · Yaozhu Wang · Shurong Xie · Xiaoyan Tang · Changxun Yu · Zhi Song

Received: 16 July 2006 / Accepted: 23 October 2006 / Published online: 6 December 2006

Abstract The mineralogy and geochemistry of the waste rocks distributed at Taojiang Mn-ore deposit, central Hunan province, China, were studied using X-ray powder diffraction (XRD), electron microprobe analysis (EMPA) fitted with energy dispersive spectrometer (EDS) and inductively coupled plasma mass spectrum (atomic emission spectra) ICP-MS (AES), with the aim of predicting the environmental impacts of weathering of the waste rocks. The mineralogical results from microscope observation and XRD and EMPA studies show that the waste rock is composed of black shale and minor Mn carbonates. The oxidation of sulfide minerals such as galena, pyrite and chalcopyrite is accompanied by decomposition of Mn carbonates and K-feldspar during exposure to atmospheric O_2. The geochemical characteristics of major, rare earth elements (REE) and trace elements of the waste rocks also show that the waste rock can be divided into black shale and Mn carbonate, and both of them are currently under chemical weathering. The major alkalies and alkaline elements (Ca, Mg, Na, K, Rb, Sr and Cs) and major elements (Fe, S and P) and heavy metals (Sc, V, Cr, Th, U, Sn, Co, Ni, Cu, Zn, Pb, Mo, Cd, Sb, an Tl) are being released during weathering. The mobility of alkalis and alkaline elements Ca, Mg, Na, K, Rb, Sr and Cs is controlled by decomposition of Mn carbonates. The dispersion of Cr, Sc and Th (U) might be related to weathering of K-feldspar, and the release of the heavy metals Co, Ni, Cu, Zn, Pb, Mo, Cd Sb and Tl is dominated by the breaking of sulfide minerals. The REE of the waste rocks and surrounding soils and the spidery distribution patterns of heavy metals in the waste rocks, the surrounding soils and the surface waters show that weathering of the waste rocks and bedrock might be the sources of heavy metal contamination for the surrounding soils and surface water system for the mining area. This is predicted by the mass-balance calculation by using Zr as an immobile element. Therefore, it is urgently necessary take measures to treat the waste rocks distributed throughout the area for the local environmental protection.

Keywords Waste rock · Chemical weathering · Heavy metals · Environmental impact · Black shale · Taojiang Mn-ore deposit

B. Peng (✉) · Y. Wang · S. Xie · X. Tang · C. Yu
Faculty of Resource and Environment Science,
Hunan Normal University, 410081 Changsha, China
e-mail: pengbo@hunnu.edu.cn; 666pengbo@sina.com.cn

A. Piestrzynski · J. Pieczonka
Ore Geology Department,
AGH University of Science and Technology,
30-059 Cracow, Poland

M. Xiao · Z. Song
Xiangya 3rd Hospital, Central-South University,
410013 Changsha, China

Introduction

In many cases, waste rock produced by mining contains an abundance of sulfide minerals of little economic value (Fanfani et al. 1997; Frostner and Wittman 1981; Moncur et al. 2005). Oxidation of the sulfide minerals such as pyrite, pyrrhotite, sphalerite, chalcopyrite and galena is responsible for the dispersion of heavy metals to environments (Nesbitt and Muir 1994; Audry et al. 2005; Lu et al. 2005; Moncur et al. 2005; Malmstrom et al. 2006). The heavy metals constitute one of the

most insidious and dangerous pollutants known to humans (Chon et al. 1996; Nurnberg 1984; Akpan et al. 2002; Lakhan et al. 2002; Peng et al. 2004). Therefore, the heavy metal contamination caused by waste rock should be an important environmental concern. Previous studies have shown that the magnitude of heavy metal contamination from waste rock is often considerable (Fanfani et al. 1997; Larocque and Rasmussen 1998; Holmstrom et al. 1999; Silva et al. 2004), and the geological perspective on the toxicity of waste rock produced from both open-pit and/or underground workings should be stressed (Fanfani et al. 1997; Larocque and Rasmussen 1998; Silva et al. 2004; Jung et al. 2005; Lu et al. 2005).

The extent and degree of heavy metal contamination around a waste rock depends upon the minerals occurring in, and the chemical characteristics of, the waste rock (Silva et al. 2004), which is composed of mostly the ore host rocks. In many places of the world, black shale hosts a remarkable array of ore deposits including Ni, Au, U, V, Se, Mn and P (Coveney et al. 1994; Emsbo et al. 2005). Continuous mining in the black shale has led to the production of an immense quantity of black-shale waste rocks. The black shale formed under anoxic deposition conditions usually contains abundant sulfide minerals and has a high concentration of many metals such as As, Cd, V, U, Cu, Pb, Zn, Hg, Mn, Mo and Ni (Jaffe et al. 2002; Peng et al. 2005). Weathering of black shale releases heavy metals such as Co, Ni, Zn, Cd, Sn, Sb, Pb and U (Peng et al. 2004), and Re and platinum group elements (Petsch et al. 2000; Peucker-Ehrenbrink and Hannigan 2000). Therefore, black shale is considered to be an important source of heavy metal contamination (Pasava et al. 2003; Peng et al. 2004; Lavergren 2005) that might cause very serious environmental problems (Peng et al. 2004). The emission of heavy metals from a waste rock is somehow controlled by the mobility of the metals during weathering. Metal mobility during weathering is ambiguous when the waste rock contains various amounts of carbonates. Lapakko et al. (1997), Blowes et al. (1998) and Holmstrom et al. (1999) deduced that high amounts of carbonate within a waste rock might reduce the concentrations of released metals, because manganese oxides formed from carbonate oxidation might act as barriers for the metal mobility due to their high sorption capacity for many heavy metals such as Cu, Co, Ni, Pb, Zn, Mo, etc., through isomorphic substitution, adsorption (ion exchange) and specific affinity (Neaman et al. 2004). However, Evangelou and Huang (1994) and Dold and Fontbote (2002) suggested that carbonates might accelerate the emission of metals through promoting oxidization of sulfides by the CO_3 produced from carbonate oxidation, during which the electron transfer via surface Fe–CO_3 complexes occurs. Therefore, it is important to understand the mobility of metals during waste rock weathering for us to predict the toxicity of a carbonate-bearing waste rock.

Central Hunan is one of the major Mn-ore producers in the People's Republic of China (Kuang et al. 2003). There are many Mn ore deposits distributed in the area, and the total unearthed Mn reservoir is more than 2×10^6 tons (Kuang et al. 2003). Theexploitation of Mn in the area was started in 1960 (Sun 1995), and waste rock piles have developed since then. The Mn-ores, mostly the Mn carbonates, are hosted in black shale of the Ordovician age (Zhu 1996), and waste rocks produced during mining in the area are always composed of black shale with Mn carbonates. The annual average minimum and maximum temperatures for the area are 16 and 30°C, respectively, and the average annual rainfall is about 1,600 mm (Peng et al. 2004), conditions that are favorable for chemical weathering. The area has recently been opened for tourism development, and the population growth for the area has doubled since 1980. However, there are a paucity of environmental assessments of the area and a lack of studies about how the waste rocks distributed throughout the area impact on the environment. The purpose of the present study is to address this lack.

Site description

The Taojiang Mn-ore deposit is located at about 25 km southwest of the Taojiang county town in central Hunan (Fig. 1a). The ores are stratigraphically bounded by the Moudaoxi formation of the middle Ordovician (Zhu 1996; Fan et al. 2004), which is composed of black shale. The outcrop of the Moudaoxi formation is controlled by many folds and is distributed sinuously throughout the mine district (Fig. 1a). The thickness of the Mn-ore-hosted black shale varies from 5 to 100 m, with an average of about 40 m. The black shale beds, from 1 to 4 m in thickness, are composed of major illite, chlorite, quartz, K-feldspar and minor pyrite, sericite, calcite, kutnohorite and organic matter (Rao and Fan 1990; Zhu 1996; Wu and Cao 2003). The pyrite in black shale ranges from more than 1 to 14%, with an average of 7%, and usually occurs as individual pyrite grains, pyrite spheralites and polyframboidal pyrites (Rao and Fan 1990). The organic matter in black shale is mostly organic carbon, 3.6% on average (Rao and Fan 1990).

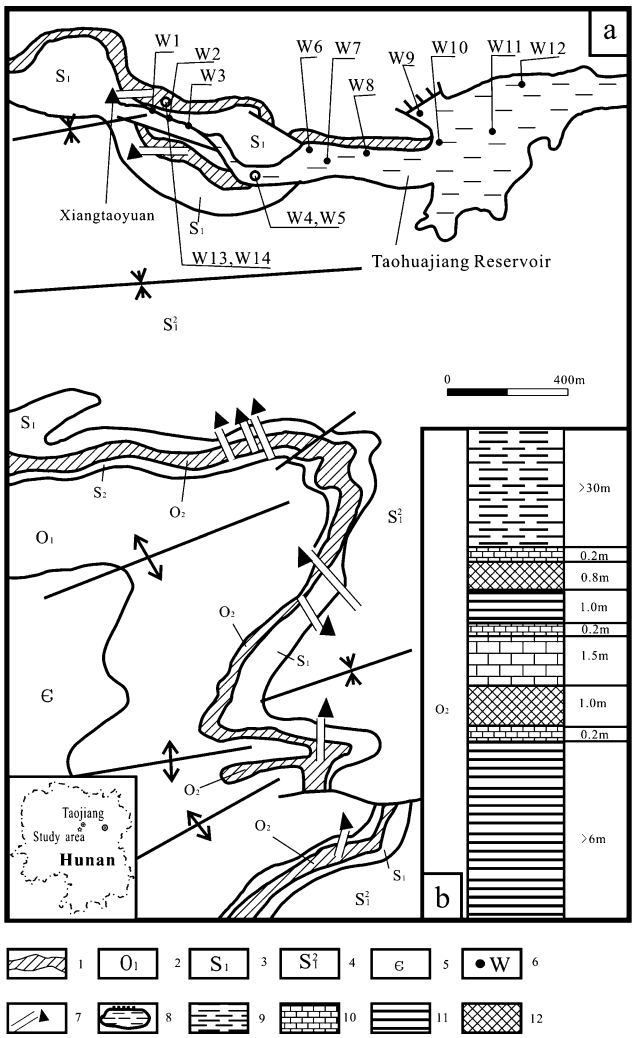

Fig. 1 Geological sketch of the Taojiang Mn ore deposit (**a**) and geological section of the ore host rock (**b**). *1* The ore-host rock (the black shale of the middle Ordovician); *2* the lower Ordovician; *3* the lower Silurian; *4* the middle Silurian; *5* the Cambrian; *6* sample location; *7* site of waste rock pile; *8* water reservoir; *9* claystone; *10* limestone; *11* black shale; *12* Mn-ore layer

There are two layers of ores hosted within the black shale, as shown in the stratigraphic profile (Fig. 1b). Each ore layer consists of four to eight interlayed monolayers of Mn ore veins. The thickness of each ore monolayer varies from 0.6 to 1.4 m, with an average of approximately 1.0 m. The ore bodies extend about 11 km throughout the mining district (Fig. 1a) and are dominated by Mn carbonates, with minor Mn oxides and Mn silicates. The minerals for the Mn carbonates include major (more than 90% in total) rhodochrosite, kutnohorite, calcite rhodochrosite and calcite, with minor (less than 10%) quartz, ankerite, sericite, chlorite, barite, pyrite, pyrrhotite, galena, sphalerite, chalcopyrite and organic matter (Rao and Fan 1990). The average concentration of Mn in carbonate ores is about 16.78%, but reaches more than 45% for the Mn oxide ores (Jiang et al. 1995; Zhu et al. 1998; Wu and Cao 2003). However, the total Mn reserve from the Mn-oxide ores is less than 8%. The waste rock in most causes did not contain the original Mn-oxide ores, and the Mn oxides found in the waste rock might be owing to later (since exposure to the atmosphere) oxidation of the Mn carbonates.

The deposit was opened in 1960 and has since been continuously exploited for metal Mn. Waste rocks composed of underground workings, mostly black shale, were developed and deposited during the mining. There are many waste rock piles distributed throughout the mining district. The one selected for this study is located at the Xiangtaoyuan mine, in the northern part of the mining district (Fig. 1a). The reason for the choice is that it is located at the end of the Taohuajiang reservoir (Fig. 1a), the water of which might contain leachates directly from the waste rock. The Mn ores (carbonates) are easily identified by their fleshy, grey and/or grey white colors, as well as their textures, and were not so easy toabandon as waste rocks during mining. Under the waste rock, there is a layer of yellowish soil developed directly on the bedrock (black shale).

Materials and methods

The waste rock, the bedrock (the ore host rock), the surrounding soils and the surface water were sampled during field investigation. Eight waste rock samples were carefully selected from the surface of the selected waste rock pile, so that the selected specimens represented all different rock types with different weathered degrees determined by colors and textures. Detailed descriptions of the waste rock samples are summarized in Table 1. Although the waste rock pile was deposited about 40 years ago, samples from the surface of it might represent waste produced in recent years and might have been exposed to the atmospheric O_2 for a short temporal span.

The mineralogy for a waste rock is complex and multiphased, and probably is a function of the local and regional climate and the time period of exposure, as suggested by Boulet and Larocque (1988). For comparison, two bedrock (host rock) samples were also selected from the geological site. One (T-2) represents the fresh bedrock, the black shale, while the other (T-3) represents the weathered bedrock. Descriptions of them are also included in Table 1. The surrounding soil samples were collected at the same

Table 1 Description of samples from waste rock at the Xiangtaoyuan mine

Sample	Description
M-1	Grey-white, Mn carbonate with minor Mn oxides developed slightly on the surface of specimen, no sulfide mineral observed, brecciated structure without change of texture and hardness, moderately weathered
M-2	Black or grey-black shale, outline of the specimen not very clear, no sulfide mineral observed on the surface, texture and hardness not changed, incipiently weathered
M-3	Black shale, outline of the specimen unclear, no sulfide mineral observed on the surface, texture and hardness not changed, incipiently or weakly weathered
M-4	Brown-black shale, outline of the specimen completely unclear, no sulfide mineral observed on the surface, texture and hardness start to change, weakly weathered
M-5	Brown-black shale, outline of the specimen completely unclear, no sulfide mineral observed on the surface, texture not changed, but the specimen showing the feature of being easily broken, weakly or moderately weathered
M-6	Brown-black and red-brown shale, outline of the specimen completely changed, Fe oxides developed on the specimen's surface, texture and hardness changed, moderately or intensively weathered
M-7	Yellowish-brown shale, outline, texture and hardness of the specimen completely changed, but no fibrous root developed, moderately or completely weathered
M-8	Soils developed not directly from the waste rocks, but from the host rock, and located directly down the waste rock pile, fibrous root developed
T-2	Black shale, bedrock and host rock for the mine, pyrite of fine grain size (less than 0.5 mm in diameter) spread on the specimen's surface, fresh rock
T-3	Black shale, similar to sample T-2

time. About 1.5 kg of each rock and soil sample was collected in clear plastic boxes.

All rock samples were firstly separated for mineralogical and geochemical studies. The Mn-ore sample M-1 was subject to the X-ray powder diffraction (XRD) analysis and electron microprobe analysis (EMPA) fitted with an energy dispersive spectrometer (EDS), after being studied under a reflecting light microscope. The powdered XRD analysis was made using a DRON-1 diffractmeter and filtered CuKα radiation, while the EMPA was carried out using the machine HITACHI-S-4700 FESEM under 20 Kv of acceleration at the Institute of Geoscience, Jagiellonian University, Poland. All other waste rock samples were subjected to electron microprobe analysis, which was carried out using the Jeol-753 Superprobe at the Ore Geology Department, AGH University of Science and Technology, Poland. The EMPA was carried out under the following environments: the accelerating voltage of 20 kV and sample current of 15 nA. The following standards and spectral lines were used: Ca Kα($CaCO_3$), O Kα (quartz), W Lα (100%), Mn Kα (100%), Mo Lα (100%), Mg Kα ($MgCO_3$), Ni Lα (100%), As Lα (InAs), Fe Kα (iron), S Kα (100%), Sb Lα (100%), Zn Kα (100%), Cu Kα (100%), Pb Mα (100%), Hg Lα (HgS).

For the geochemical study, the separated rock and soil samples were powdered in an Alceramic shatter box after drying at 100°C for 3 h in a laboratory. All analytical data were reported on a dry sediment basis. About 50 mg of powder from each sample was dissolved using HF + HNO_3 solution in a disposable platinum crucible to oxidize the organic matter. The dissolved sample was then diluted using 2% HNO_3, and major elements were analyzed using an Elan6000 ICP-AES machine at the Guangzhou Institute of Geochemistry, the Chinese Academy of Science. Then a number of heavy metals, trace elements and REE were analyzed at a wide range of concentrations with high accuracy using an Elan6000 ICP-MS machine at the same institute.

Surface water samples for this study included three from a stream (W1, W2, W3) that runs directly down to the Taohuajiang reservoir and might contain leachates from the waste rocks, two from the tap-water system (W4, W5) that supplies water for the mine through pumping water at a upward site of the reservoir, seven from the Taohuajiang reservoir (W6–W12) and two from a fountain (W13, W14) derived from a deep part of the crust through a fault. The water sample locations are shown in Fig. 1a. The pH values of the selected waters were firstly determined during sampling, and then each 1-l water sample was collected in a clear plastic bottle and acidified in situ with HNO_3. All the water samples were then filtrated with 0.45-μm Millipore filters in a laboratory and analyzed for a large number of elements using the Elan6000 ICP-MS machine at the Guangzhou Institute of Geochemistry.

Results

Mineralogy

The results of EMPA together with EDS on waste rocks are summarized in Tables 2 and 3. The microscope studies showed that eight waste rock samples included one Mn carbonate (MWR) and seven black shales (BWR). Their mineralogyis described as follows.

Table 2 Electron microprobe analyzing results for Mn-ore waste rock sample (M-1)

Phase	Point	Element	Atom%[a]	Element (wt%)	Rrr (1-δ)	Formula	Wt%
$MnCO_3$	M1/1-1	Ca	5.9	4.37	0.2	$MnCO_3$	
		Mn	94.1	95.63	1.01		
$(CaMn)CO_3$	M1/1-2	Ca	3.16	3.61	0.15	CaO	5.06
		Mn	46.84	73.53	1.31	MnO	94.94
		O	50.0	22.86	0.6	F	0.81
		F	1.49	0.81	0.08	CaO	5.1
		Ca	3.16	3.64	0.69	MnO	94.09
		Mn	46.1	72.87			
		O	49.25	22.68			
	M1/2-1	F	0.0	0.0	0.01	F	0
		Mg	0.63	0.44	0.09	MgO	0.72
		Ca	2.9	3.22	0.09	CaO	4.5
		Mn	46.57	73.4	0.83	MnO	94.77
		O	50.0	22.95			
	M1/2-2	Ca	5.35	6.18	0.2	CaO	8.65
		Mn	44.65	70.74	0.85	MnO	91.35
		O	50.0	23.07			
	M1/2-3	Ca	2.37	2.7	0.09	CaO	3.78
		Mn	47.63	74.52	0.82	MnO	96.22
		O	50.0	22.78			
$Mn(OH)_2$/MnO	M1/1-3	Mg	8.29	7.05	0.2	MgO	11.69
		Ca	29.28	41.06	0.43	CaO	57.45
		Mn	12.43	23.9	0.65	MnO	30.86
		O	50.0	27.99			
	M1/1-4	Mg	5.34	4.38	0.13	MgO	7.26
		Si	1.34	1.27	0.08	SiO_3	2.72
		Ca	22.12	29.86	0.36	CaO	41.78
		Mn	17.18	31.79	0.71	MnO	41.05
		Fe	2.68	5.04	0.55	$Fe2O_3$	7.2
		O	51.34	27.67			
	M1/1-5	Mg	10.53	9.29	0.22	MgO	15.41
		Al	0.51	0.5	0.09	Al_2O_3	0.94
		Si	0.5	0.51	0.08	SiO_2	1.08
		Ca	27.77	40.41	0.43	CaO	56.54
		Mn	8.13	16.21	0.59	MnO	20.93
		Fe	1.75	3.56	0.49	Fe_2O_3	5.09
		O	50.81	29.52			
	M1/2-4	Mg	6.56	5.49	0.23	MgO	9.1
		Ca	28.56	39.39	0.5	CaO	55.11
		Mn	12.74	24.08	0.8	MnO	31.1
		Fe	1.71	3.28	0.62	Fe_2O_3	4.69
		O	50.43	27.76			
	M1/2-5	Mg	11.46	10.14	0.28	MgO	16.81
		Ca	29.22	42.61	0.54	CaO	59.61
		Mn	6.83	13.65	0.73	MnO	17.63
		Fe	1.9	3.87	0.64	Fe_2O_3	5.53
		Sr	0.11	0.36	0.2	SrO	0.42
		O	50.48	29.38			
Sulfide	M1/1-6	S	53.2	38.56	0.31	NiS	
		Ca	0.89	0.8	0.07		
		Mn	3.58	4.44	0.31		
		Co	0.58	0.77	0.18		
		Ni	41.75		0.83		
	M1/1-7	S	53.13	38.39	0.31	NiS	
		Mn	4.7	5.81	0.33		
		Ni	42.17	55.8	0.85		
	M1/3-1	S	44.97	11.74	0.49	PbS	
		Mn	3.71	1.66	0.22		
		Pb	51.32	86.6	3.14		

Table 2 continued

Phase	Point	Element	Atom%[a]	Element (wt%)	Rrr (1-δ)	Formula	Wt%
	M1/3-2	Mn	10.42	4.33	0.58	PbS	
		Pb	55.88	87.51	5.79		
		S	33.7	8.17	0.73		
	M1/3-3	Mg	0.62	0.16	0.13	PbO	
		Cd	0.37	0.44	0.39	MnO	
		Ca	2.87	1.23	0.13		
		Mn	70.61	41.53	0.9		
		Pb	25.53	56.63	3.44		
		Mg	0.64	0.17	0.12		
		Cd	0.35	0.43	0.39		
		Ca	2.79	1.22	0.13		
		Mn	68.74	41.14	0.89		
		Pb	24.87	56.14	3.41		
		S	2.6	0.91	0.52		
	M1/3-4	S	37.66	10.38	0.62	PbS	
		Ca	3.03	1.04	0.15		
		Mn	13.02	6.15	0.65		
		Pb	46.29	82.43	5.82		

[a] ZAF correction

Table 3 Electron microprobe analyzing results (wt%) for sulfide minerals in waste rock and bed rocks

Sample	Point	Fe	S	Co	Ni	Cu	Au	Ag	Mineral
M-5	AP9-3/1	39.69	38.13	0.14	0.07	0.04	0.03	0.04	py
M-6	AP9-1/1	47.76	50.22	0.12	0.01	0.02	0.03	0.04	py
	AP9-1/2	47.29	51.85	0.06	0.12	0.02	0.04	0.04	py
	AP9-1/3	47.69	50.61	0.06	0.02	0.02	0.03	0.04	py
	AP9-1/4	48.38	50.99	0.05	0.02	0.02	0.04	0.04	py
	AP9-2/1	48.53	51.93	0.08	0.03	0.02	0.003	0.04	py
	AP9-2/2	47.61	51.39	0.09	0.01	0.02	0.03	0.04	py
Average		40.88	43.34	0.076	0.04	0.023	0.029	0.04	$Fe_{0.73}$ $S_{1.35}$
M-6	AP9-1/5	30.55	34.46	0.06	0.01	35.9	0.08	0.04	cpy
	AP9-1/6	31.52	34.4	0.08	0.01	35.75	0.03	0.04	cpy
T-2	AP8-3/1	46.07	53.87	0.08	0.01	0.02	0.03	0.04	py
	AP8-3/2	46.29	53.53	0.03	0.03	0.03	0.03	0.04	py
	AP8-3/3	46.17	53.66	0.09	0.19	0.02	0.03	0.04	py
	AP8-3/4	45.43	53.9	0.07	0.07	0.02	0.03	0.04	py
	AP8-3/5	43.55	53.93	0.12	0.01	0.8	0.07	0.04	py
	AP8-3/6	44.57	54.05	0.14	0.17	0.02	0.04	0.04	py
	AP8-4/1	46.63	54.57	0.03	0.01	0.02	0.03	0.04	py
	AP8-4/2	45.85	54.51	0.08	0.01	0.02	0.03	0.04	py
	AP8-4/3	46.02	53.99	0.11	0.01	0.02	0.03	0.04	py
Average		45.62	54.00	0.083	0.057	0.108	0.036	0.04	$Fe_{0.82}S_{1.684}$

py Pyrite; *cpy* chalcopyrite; *om* organic matter

Mn-ore waste rock

The X-ray powder diffraction (XRD) analysis was firstly applied to the MWR (M-1) and showed that the MWR contains major rhodochrosite ($MnCO_3$), kutnohorite [$(Ca_{0.97}Mn_{0.5}Mg_{0.5})CO_3$], hausmannite ($Mn_3O_4$), manganosite (MnO), wodginite [$(TaMnSn)O_2$], feitknechtite (MnOOH) and minor quartz (SiO_2). Among these minerals, the kutnohorite, rhodochrosite and quartz may represent the original mineral phases for MWR, and the hausmannite, manganosite, wodginite and feitkechtite may be the products from oxidizing the above original carbonate minerals, possibly through the following chemical reactions:

$$MnCO_3(\text{rhodochrosite}) + H_2O + CO_2 = Mn(HCO_3)_2 \quad (1)$$

$$Mn(HCO_3)_2 = MnO(\text{manganosite}) + 2CO_2 + H_2O \quad (2)$$

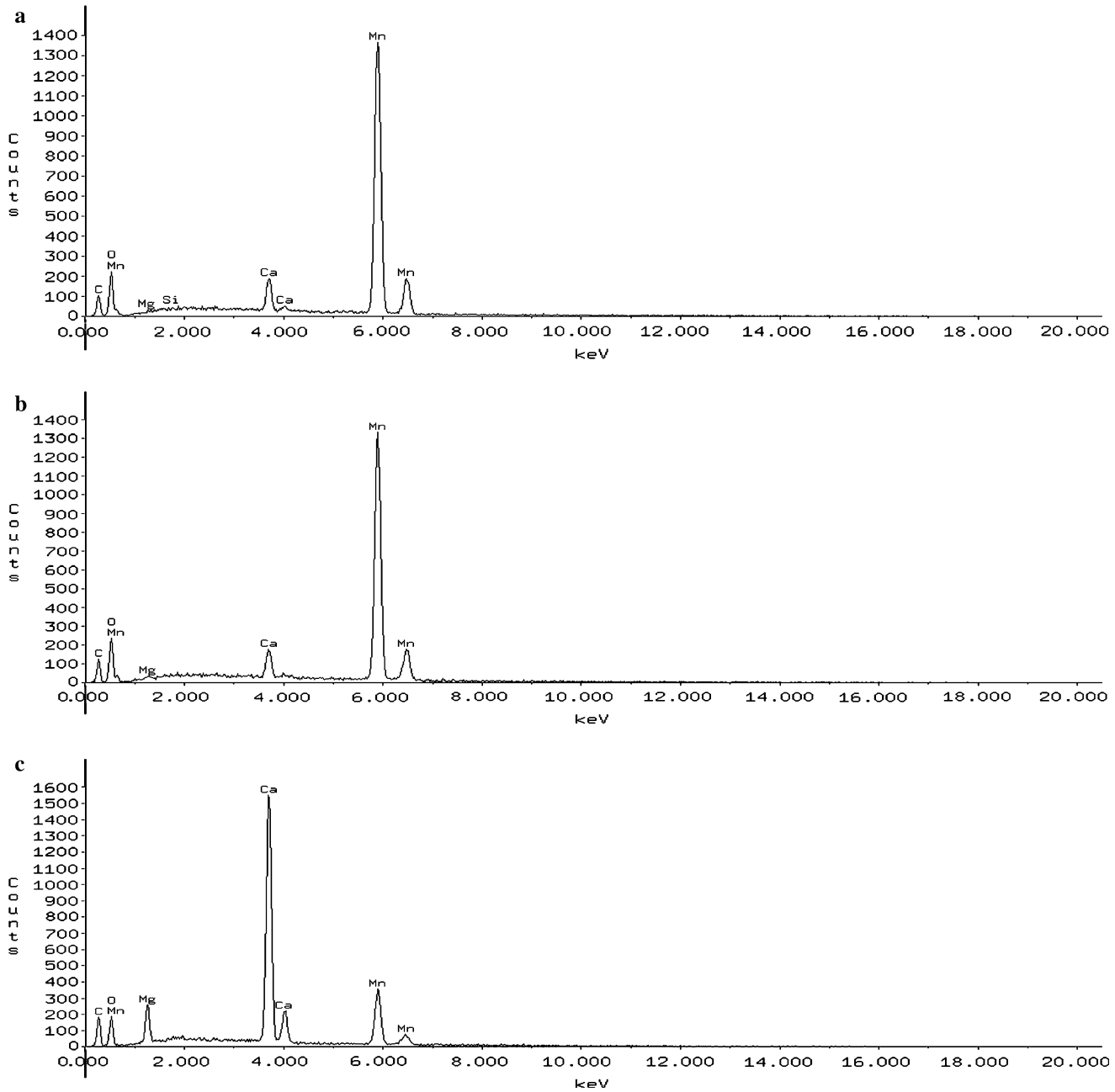

Fig. 2 EDS spectra of different minerals hosted within the Mn-carbonate waste rocks. For details, see the text

$$\mathrm{Mn(HCO_3)_2 + 2OH^- + 2H^+ = Mn(OH)_2(feiknechtite) + 2CO_2 + 2H_2O} \quad (3)$$

$$\mathrm{6Mn(OH)_2 + O_2 = 2Mn_3O_4(hausmannite) + 6H_2O} \quad (4)$$

$$\mathrm{Mn_3O_4(hausmannite) + O_2 = 3MnO_2(wodginite).} \quad (5)$$

Under the electron microscope, it was seen that the MWR contains Mn carbonates, Mn oxides and sulfide minerals. The Mn carbonates were oxidized to some extent. The fresh carbonate has awhite or grey white color with higher reflected light; however, the oxidized carbonate is mostly grey or dark grey with much lower reflected light. The EDS results (Table 2) show that the Mn concentration in fresh carbonates is up to 95.63%, with Ca at 4.37%. Combining the XRD results and EDS analyses (Fig. 2a), it was deduced that the fresh carbonate (M1/1-1; Table 2) may be rhodochrosite, with the chemical formula $MnCO_3$. However, the concentration of Mn (from four other analyzed points) in oxidized carbonates ranges from 70 to 74%, with an

Table 4 Concentrations of major elements (%), trace elements (ppm) and rare earth elements (ppm) of waste rock and bedrock at the Xiangtaoyuan mine

Sample	M-1	M-2	M-3	M-4	M-5	M-6	M-7	M-8	T-2	T-3	BWR[a]	MC[b]	BS[c]
Major and trace elements													
SiO_2	28.30	59.54	62.70	54.71	58.68	49.66	69.07	61.42	58.76	67.14	59.40	12.30	67.00
TiO_2	0.37	0.69	0.74	0.84	0.71	0.68	0.63	0.88	0.80	0.70	0.74	0.27	0.20
Al_2O_3	5.76	17.73	14.49	13.69	17.71	16.08	14.41	14.34	17.23	15.29	15.49	2.93	8.60
Fe_2O_3	4.74	8.55	5.75	5.79	8.68	9.93	5.20	5.10	5.82	5.47	7.00	3.97	4.10
MnO	28.01	0.10	0.83	6.55	0.08	0.30	0.04	1.56	0.06	0.07	1.35	28.17	0.01
MgO	4.22	2.77	5.71	3.45	2.75	1.85	1.33	1.45	2.59	1.61	2.76	2.71	1.00
CaO	16.78	0.30	0.86	2.07	0.20	4.74	0.23	1.80	0.51	0.41	1.46	19.98	1.40
K_2O	1.91	4.72	3.02	3.29	4.67	4.16	3.12	2.94	4.47	3.22	3.70	0.70	2.60
Na_2O	0.03	0.80	1.13	0.76	0.87	1.26	1.07	0.49	1.06	1.71	0.91	0.33	0.30
P_2O_5	0.15	0.09	0.06	0.07	0.10	0.14	0.09	0.21	0.14	0.19	0.109	0.04	0.70
Ig[d]	10.51	5.13	5.34	9.02	5.14	11.71	3.90	8.99	7.99	4.15	7.03	10.49	
Total	100.80	100.42	100.63	100.20	99.59	100.51	99.09	99.18	99.43	99.96	99.95	99.81	
Al_2O_3/SiO_2	0.20	0.30	0.23	0.25	0.30	0.32	0.21	0.23	0.29	0.23	0.26	0.24	0.13
K_2O/Na_2O	63.67	5.90	2.67	4.33	5.37	3.30	2.92	6.00	4.22	1.88	4.06	2.12	8.67
$Al_2O_3/(Na_2O + CaO)$	0.34	16.12	7.28	4.84	16.55	2.68	11.08	6.26	10.98	7.21	6.54	0.14	5.10
Al_2O_3/K_2O	3.02	3.76	4.80	4.16	3.79	3.87	4.62	4.88	3.85	4.75	4.18	4.186	3.31
Al_2O_3/Na_2O	192.00	22.16	12.82	18.01	20.36	12.76	13.47	29.27	16.26	8.94	17.00	8.88	28.67
CIA[e]	72.67	71.78	68.41	69.31	72.11	65.03	72.17	74.94	69.65	62.66	70.54		
P	700.30	421.30	290.40	335.60	440.2	638.70	412.0	930.9	655.4	877.60	495.59		700
Ba	1,315.0	1,930	2,367.8	2,994.0	1,864.3	1,844.4	2,132.0	1,666.0	1,825	3,116.0	2,114		550
Ti	2,219.0	4,054	4,335.9	4,778.0	4,187.1	4,052.3	3,754.0	5,092.0	4892.4	4,128.5	4,321.8		4,600
Zr	63.38	62.82	116.50	139.30	80.96	81.44	100.10	122.9	95.67	79.55	100.57		160
Hf	1.765	1.863	2.898	3.016	1.901	1.993	2.765	3.365	2.882	2.643	2.54		2.8
Nb	12.01	13.88	15.95	21.77	14.44	15.47	13.53	19.13	17.99	14.53	16.31		18
Ta	0.592	1.443	1.139	1.249	1.337	1.379	1.184	1.421	1.697	1.429	1.307		2
Ga	14.52	25.20	21.23	21.38	25.17	23.63	16.89	20.49	23.56	19.62	21.998		23
Ge	0.541	1.47	1.523	0.469	1.53	1.39	1.264	1.40	1.362	1.401	1.292		6
Rb	78.58	199.40	130.30	151.50	194.2	192.0	141.90	148.60	200.30	151.4	165.41		160
Sr	1,114.3	87.83	116.20	142.80	84.30	357.9	63.81	169.10	102.10	70.97	145.99		300
Cs	3.144	39.40	30.16	23.17	35.22	30.69	14.79	15.04	15.212	12.30	26.92		5.5
Y	29.43	21.02	16.60	20.56	22.16	40.69	28.16	29.50	27.74	37.56	25.53		41
Zr/Hf	35.91	33.72	40.20	46.19	42.59	40.86	36.20	36.52	33.20	30.10	39.47		
Nb/Ta	20.29	9.62	14.00	17.43	10.80	11.22	11.43	13.46	10.601	10.17	12.57		
Zr/Nb	5.28	4.53	7.30	6.40	5.61	5.26	7.40	6.42	5.32	5.47	6.13		
Rare earth elements													
La	56.26	46.99	45.57	50.31	46.81	57.85	46.37	54.59	57.87	52.22			
Ce	161.60	89.28	94.71	91.84	89.15	115.90	86.83	111.20	106.7	95.38			
Pr	11.32	10.47	10.03	9.031	10.30	14.02	11.03	12.04	12.29	12.22			
Nd	43.47	37.23	35.63	31.16	37.62	51.89	41.25	44.18	44.01	46.60			
Sm	7.68	6.426	5.851	5.13	6.506	9.83	7.349	7.35	7.349	9.109			
Eu	1.419	1.214	1.038	1.016	1.21	2.142	1.447	1.458	1.245	1.846			
Gd	7.583	5.329	4.517	4.593	5.42	9.045	6.356	6.575	6.026	8.765			
Tb	1.123	0.826	0.665	0.693	0.837	1.44	1.036	1.021	0.942	1.391			
Dy	5.956	4.441	3.711	3.833	4.561	7.461	5.593	5.576	5.25	7.769			

Table 4 continued

Sample	M-1	M-2	M-3	M-4	M-5	M-6	M-7	M-8	T-2	T-3	BWR[a]	MC[b]	BS[c]
Ho	1.154	0.827	0.701	0.795	0.861	1.475	1.088	1.10	1.054	1.522			
Er	3.285	2.367	2.183	2.33	2.468	4.14	3.079	3.244	3.20	4.174			
Tm	0.498	0.363	0.343	0.358	0.379	0.657	0.456	0.489	0.518	0.623			
Yb	3.192	2.332	2.482	2.518	2.448	4.326	2.921	3.225	3.502	3.975			
Lu	0.489	0.36	0.413	0.389	0.378	0.695	0.459	0.48	0.566	0.615			
∑REE	305.0	208.5	207.84	204	208.95	280.87	215.30	252.50	205.52	246.21			
LREE/ HREE	3.59	1.47	1.16	1.32	1.35	2.03	1.01	1.27	1.25	1.05			
$(La/Yb)_n$	9.88	11.42	10.40	11.32	10.84	7.58	8.99	9.59	9.36	7.04			
$(La/Sm)_n$	5.13	5.12	5.45	6.87	5.04	4.12	4.12	5.20	5.51	4.01			
$(Gd/Yb)_n$	1.26	1.21	0.97	0.97	1.18	1.11	1.16	1.08	0.91	1.17			
Heavy metals													
Sc	4.446	18.08	13.21	10.38	17.56	15.53	10.65	11.07	16.15	12.07	13.78		
V	160.30	105.10	106.10	191.30	107.60	437.60	141.70	122.80	761.30	98.29	173.17		
Cr	31.28	93.01	61.83	72.19	94.48	76.80	64.15	65.98	94.31	65.77	75.49		
Mn	-	395.60	5,991.8	47,355	516.50	2195.9	307.60	11,115	456.90	547.50	9,696.8		
Co	193.70	53.61	33.48	58.58	28.61	53.12	12.22	33.07	29.49	19.02	38.96		
Ni	1,069	43.23	106.90	229.70	37.98	195.50	33.27	178.50	168.10	36.62	117.87		
Cu	317.20	142.10	82.72	148.30	54.10	166.70	29.54	78.35	151.90	31.17	100.26		
Zn	379.70	197.30	148.0	284.50	87.22	375.90	80.90	227.80	397.20	68.23	200.23		
Pb	137.90	26.23	11.70	39.61	41.28	140.70	22.05	82.75	39.90	16.39	52.05		
Th	11.54	19.02	17.73	18.01	18.71	23.93	18.51	18.20	25.70	18.98	19.16		
U	5.254	4.013	2.321	9.258	3.421	38.46	4.169	4.912	26.70	3.886	9.51		
Mo	77.15	1.839	0.842	6.056	0.945	64.74	1.381	3.22	28.79	1.094	11.29		
Cd	1.14	0.20	0.15	0.878	0.095	1.756	0.062	0.893	3.244	0.238	0.58		
Sn	6.324	12.67	9.386	13.73	10.22	9.061	7.568	10.05	10.406	10.05	10.38		
Sb	27.03	6.037	3.686	13.76	6.838	17.08	4.998	4.529	11.424	6.074	8.13		
Tl	2.048	1.23	0.754	0.936	1.134	2.106	0.79	1.022	2.182	0.825	1.14		

[a] The average value of two analyzing results for major elements with deviation in percentage less than 5%, and seven analyzing results for trace elements and rare earth elements with deviation in percentage less than 10%

[b] BWR represents average of black shale waste rock (from M-2 to M-8)

[c] MC represents regional Mn carbonate rocks after Fu (2001)

[d] BS represents average world black shales (n=34) after Mason and Morre (1982)

[e] Ig represents the amount of ignition

[f] CIA = $Al_2O_3/(Al_2O_3 + CaO^* + Na_2O + K_2O) \times 100$, where Al_2O_3, CaO, Na_2O and K_2O are in molecular proportions, if $CaO \leq Na_2O$, CaO^* is CaO, if $CaO > Na_2O$, CaO^* is represented by Na_2O for calculation

average of 73.05% (n=4; Table 2), which is much lower than in the fresh carbonate. The concentrations of Ca in oxidized carbonates are similar to those in the fresh one. The EDS results (Table 2) show that oxidized carbonates contain a definite amount of Mg and a high amount of oxygen. Also, combining the XRD and EDS results (Fig. 2b), it is estimated that the oxidized Mn carbonate probably is rhodochrosite, or kutnohorite, with the chemical formula $(Ca_{0.97}Mn_{0.5}Mg_{0.5})CO_3$ and with a high amount of oxides, probably MgO, and CaO.

The Mn oxides are monotonously black and dark, always with much lower reflected light. The EDS results show that they contain Mn, Ca, Mg and O, with minor Al, Fe, Si and Sr. The concentrations of Mn, Ca, Mg and O from five analyzed points on the Mn oxides are variable and on average are 21.93, 38.67, 7.27 and 28.45% (n=5; Table 2), respectively. It is not possible to calculate their detailed chemical forms from the EDS results, but by combining the XRD and EDS results (Table 2; Fig. 2c), it is deduced that the oxide minerals may include hausmannite and manganosite.

The sulfide minerals observed under the microscope include pyrite, galena and chalcopyrite, and millerite. The EDS results (Table 2) display the occurrence of millerite (NiS) and galena (PbS) within the MWR. The oxidizing zones developed in galena grains clearly indicate features of being oxidized. However, no evidence of oxidation was observed on millerite grains, illuminating that galena grains are easier to oxidize than millerite. The elemental composition of the oxidized galena grains is a complex mix of Pb with Mn, Mg, Cd and Ca. Compared to the stoichiometric form of galena, the element S in galena is distinctly lower, probably indicating a loss of the element S from galena during weathering.

Pyrite in pentagonal dodecahedron form was also oxidized during weathering. It should be pointed out that the occurrences of sulfide crystals and the oxidization features for galena and pyrite clearly show that the sulfide minerals hosted within the MWR are contemporaneous crystals formed during the formation of Mn carbonates, not during Mn carbonate weathering.

Black shale waste rock

The waste rock is dominated by black shale. Mineralogical study of BWR shows that the sulfide minerals within it are mostly pyrite with minor chalcopyrite. The pyrite grains are mostly in pentagonal dodecahedron form, and the polyframboidal grains, as described by Rao and Fan (1990). The EMPA results show that the pyrite contains the trace metals Co, Cu, Ni, Au and Ag, with an average content of 0.076, 0.023, 0.04, 0.029 and 0.04% (n=8; Table 3), respectively. These values are lower than the corresponding metals in pyrites of the bedrock, which average of 0.083, 0.108, 0.057, 0.036 and 0.04% (n=9; Table 3), respectively. Compared to the stoichiometric forms of pyrites (average in form of $Fe_{0.97}S_2$, n=9) in bedrock, the element S in pyrites (in average of $Fe_{1.08}S_2$, n=8) of the waste rock is distinctly lower, showing the element S was probably lost during weathering. The above EMPA results for two occurrences of pyrite suggest that the loss of the element S during weathering was accompanied by the release of other metals including Co, Cu, Ni and Au.

Geochemistry

Waste rocks

The concentrations of major elements, trace elements, REE and heavy metals of the waste rocks are listed in Table 4. In terms of major element compositions, the M-1 is characterized by low SiO_2, Al_2O_3, $Fe_2O_3^*$ + MgO, and Na_2O + K_2O (28.30, 5.76, 8.96 and 1.94%, respectively), but high MnO and CaO (28.01 and 16.78%, respectively). This is similar to that of the average Mn carbonates (MC, n=13; Fu 2001) as shown in Table 4, but distinctly different from the rest waste rocks (the BWR, e.g., M-2, M-8, etc.).

The difference of major element compositions among the sampled waste rocks also indicates the partition of MWR and BWR, as identified under the microscope. The BWR contains contents of SiO_2, TiO_2, Al_2O_3, $Fe_2O_3^*$, Na_2O and P_2O_5, with an average of 59.40, 0.74, 15.49, 7.0 0, 0.91 and 0.11%, respectively, similar to that of bedrock (T-2) and average black shales (BS, n=34; Table 4). However, the contents of MnO, CaO and MgO are variable (0.08–1.56, 0.2–4.74 and 1.33–5.71%, respectively), with an average of 1.35, 1.46, and 2.36%, respectively. These values are higher than those of the bedrock (T-2) and average black shales (n=34; Table 4) except for CaO. The contents of K_2O in BWR vary from 2.94 to 4.72%, with an average of 3.70%, similar to that of the bedrock (T-2) and weathered bedrock (T-3), but distinctly higher than that of the MWR and the average Mn carbonates (n=13; Table 4).

All the waste rocks have similar ratios of Al_2O_3/SiO_2 and Al_2O_3/K_2O, but vary in Al_2O_3/Na_2O, K_2O/Na_2O and $Al_2O_3/(Na_2O + CaO)$. The ratios of Al_2O_3/Na_2O and K_2O/Na_2O for MWR are greatly higher than BWR, but $Al_2O_3/(Na_2O + CaO)$ is lower than BWR, probably indicating that the MWR was weathered to a higher degree than the BWR. The CIA of BWR is

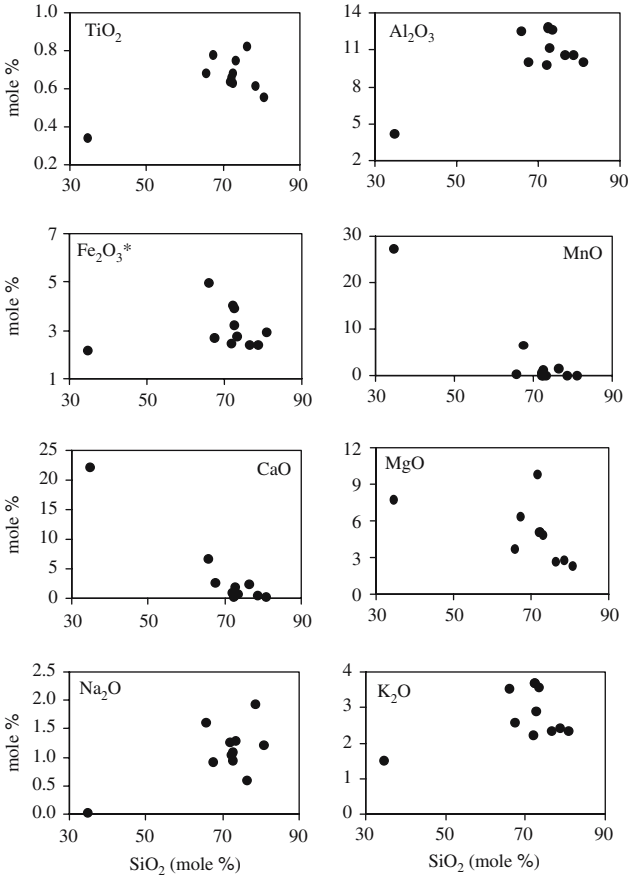

Fig. 3 Major element variation diagrams of SiO_2 versus TiO_2, Al_2O_3, Fe_2O_2, MnO, CaO, MgO, Na_2O and K_2O, respectively, of the waste rocks

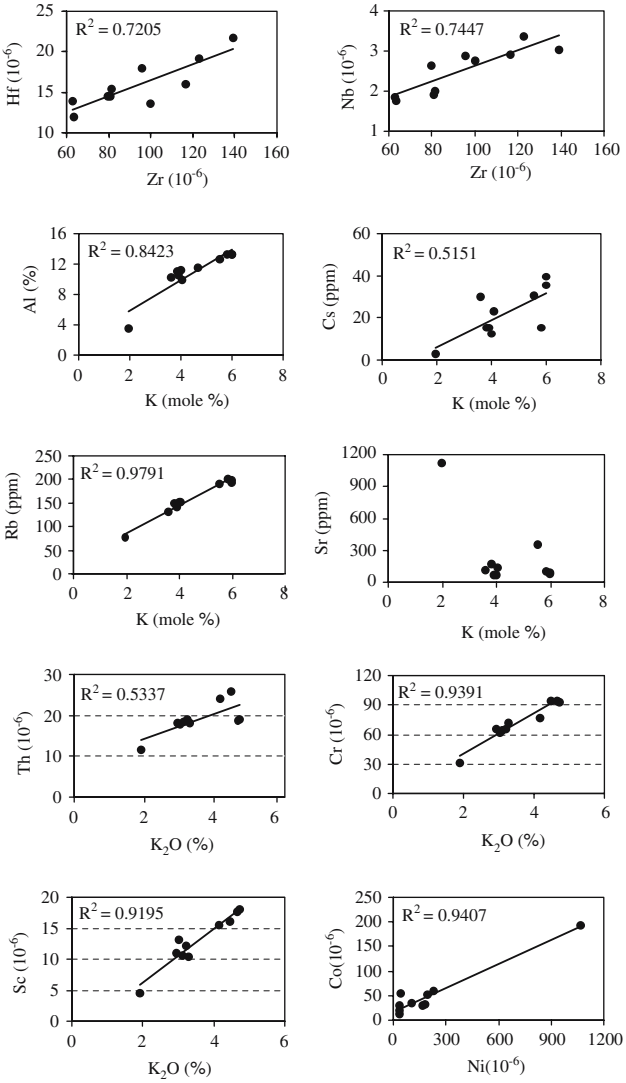

Fig. 4 Plots of trace element pairs

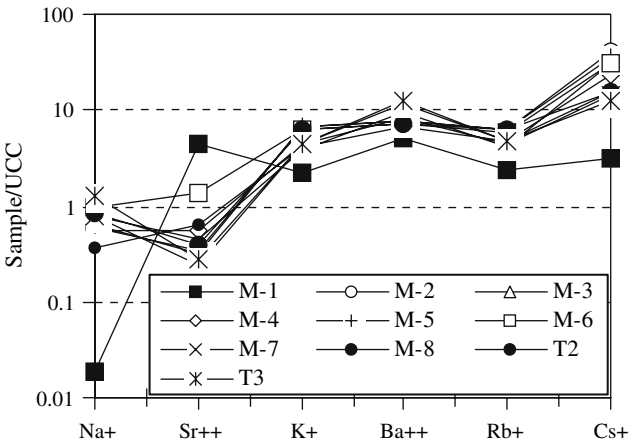

Fig. 5 Plot of major alkali and alkaline earth elements in order of increasing ionic radius for the waste rocks; *UCC* represents the upper continent crust after Taylor and Mclennan (1995)

moderate, from 62 to 74 (Table 4), suggesting that the effects of weathering had not proceeded to the stage where alkali and alkaline earth elements are substantially removed from clay minerals. It also indicates that the weathering is essentially the conversion of plagioclase to clays, or that there is a more intense decomposition of plagioclase than K-feldspar during weathering, as suggested by Nesbitt et al. (1980). Also, depletion of Na and high K_2O/Na_2O ratios of the waste rocks might have been caused by more intense decomposition of plagioclase than K-feldspar. However, the detected major element compositions of waste rocks resulted from both weathering of source rocks during sedimentation processes and the exposure weathering of waste rock due to mining.

Many studies (e.g., Bhatia 1983; Feng and Kerrich 1990) show that source weathering may cause variable degrees of negative correlations for SiO_2 versus Al_2O_3, $Fe_2O_3^*$, MgO, TiO_2 and Na_2O, and the negative correlations reflect a decrease in unstable components (e.g., feldspar) with an increase in mineralogical

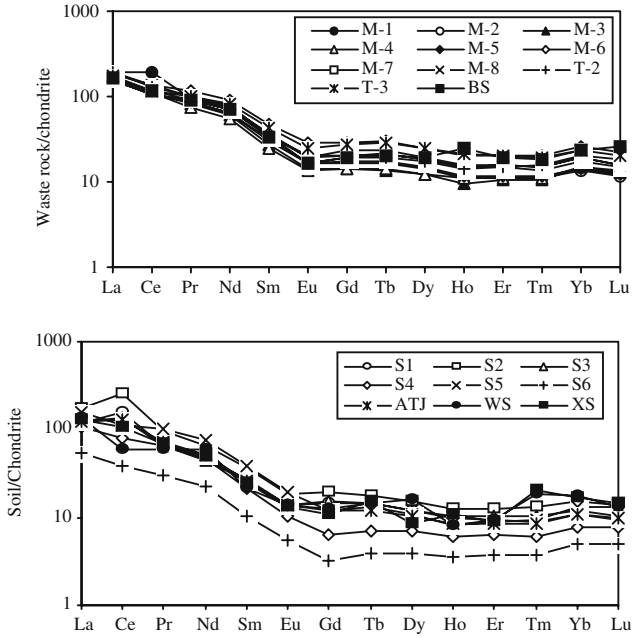

Fig. 6 Chondrite-normalized REE patterns for the watste rocks (**a**) and surrounding soils (**b**)

maturity. The present data from waste rocks do not show clearly negative corrections (Fig. 3) for SiO_2 versus Al_2O_3, $Fe_2O_3^*$, MgO, TiO_2 and Na_2O, implying that the relation of unstable components (e.g., feldspar) to mineralogical maturity is distributed. This distributed relation among SiO_2 and Al_2O_3, $Fe_2O_3^*$, MgO, TiO_2 and Na_2O probably is the result ofsecondary weathering, the exposure weathering that resulted in scatter on plots of SiO_2 versus Al_2O_3, $Fe_2O_3^*$, MgO, TiO_2 and Na_2O, as suggested by Feng and Kerrich (1990).

It is not possible to distinguish exposure weathering from source weathering for MWR and BWR by the above major element compositions. It can be deduced, however, that the exposure weathering is mostly characterized by decomposition of K-feldspar, while source weathering is characterized by decomposition of plagioclase. This agrees with Nesbitt et al.'s (1980) conclusion that Na is leached preferentially to K during chemical weathering.

The contents of P, Ba, Ti and other trace elements (Zr, Hf, Nb, Ta, Ga, Ge, Rb, Cs and Y) in MWR are consistent with the corresponding elements of BWR (Table 4). Among the trace elements, Ta, Hf, Nb and Y, in both MWR and BWR, are relatively constant, but Zr is in variable concentrations (from 62 to 139 ppm). Similar ratios of Zr/Hf and Zr/Nb (Fig. 4) indicate that Zr might be immobile during weathering. Positive correlations exist among K–Al, K–Cs and K–Rb (Fig. 4), indicating K-bearing clay minerals (e.g., illite

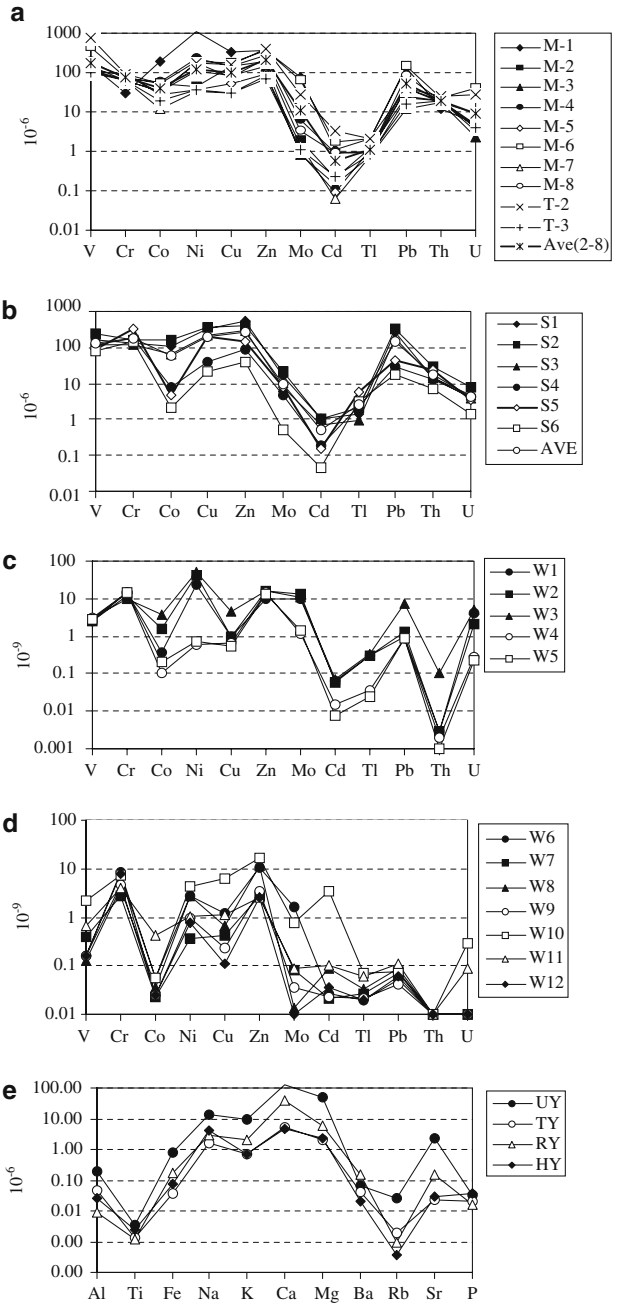

Fig. 7 Spidery diagrams for heavy metals of the waste rocks (**a**), surrounding soils (**b**) and surface waters (**c**), and for major elements of surface water (**e**)

and sericite) are probably controlling the abundances of these elements (McLennan et al. 1983). Sr is extremely enriched in MWR (M-1), but depleted to some extent in BWR. The scatter between Sr and K (Fig. 4) shows that Sr was leached from parent rocks and K was enriched (through ion-exchange) onto clays formed during the decomposition of Sr-enriched plagioclase. Concentrations of alkali and alkaline earth elements (except Ca and Mg) are normalized to the average

Table 5 Concentrations of trace metals (ppm) and rare earth elements (ppm) of the surrounding soils at Xiang Taoyuan waste rock pile

Sample	S1	S2	S3	S4	S5	S6	AVE[a]	WS[b]	XS[c]
Al	38,682.8	61,179.1	49,286.1	48,980.5	156,595.8	55,267.1	68,331.90	71,000	
Fe	24,436.1	29,201.7	29,365.2	23,590.2	34,578.9	12,955.8	25,688.0	40,000	35,000
Mn	>	>	>	383.041	69.597	30.869		1,000	441.0
V	164.90	248.90	116.20	126.00	85.672	79.092	136.79	90.0	136.0
Cr	137.60	162.60	115.60	183.70	332.20	140.50	178.70	70.0	67.0
Co	110.50	157.00	64.30	7.965	4.623	2.166	57.76	8.0	15.0
Cu	337.10	367.10	209.10	39.47	202.03	20.96	195.96	30.0	27.0
Zn	560.90	403.10	306.60	90.77	149.30	37.99	258.11	90.0	95.0
Mo	15.889	22.471	8.25	4.532	7.997	0.505	9.94	1.20	1.20
Cd	1.05	1.044	0.697	0.192	0.157	0.046	0.53	0.35	0.093
Tl	1.37	2.078	0.911	2.253	6.039	3.20	2.64	0.20	0.20
Pb	276.20	337.30	175.70	28.59	44.36	16.82	146.50	35.0	27.0
Th	13.93	29.70	14.60	12.77	22.89	6.88	16.80	9.0	16.0
U	4.589	8.008	3.892	4.144	3.522	1.423	4.26	2.0	4.2
Rb	85.38	130.82	93.83	74.37	252.40	143.80	130.10	150	–
Sr	818.90	704.30	516.80	49.86	26.16	15.64	355.28	250	250.0
Th/U	3.04	3.71	3.75	3.08	6.50	4.83	3.94	4.50	–
EI^{d}_{WS}	6.35	8.22	3.94	2.48	5.23	2.07	4.72	1.00	1.20
EI^{d}_{XW}	6.60	8.11	4.10	2.42	5.22	2.03	4.74	1.23	1.00
La	35.89	53.11	37.16	32.78	47.78	16.51	37.21	40.00	38.0
Ce	132.90	210.40	117.10	67.11	94.67	32.74	109.15	50.00	89.0
Pr	7.999	11.55	8.055	7.784	12.008	3.663	8.51	7.00	8.21
Nd	26.58	38.96	26.10	27.49	43.13	12.97	29.21	35.00	28.00
Sm	5.623	7.608	5.445	4.56	7.925	2.181	5.56	4.50	5.30
Eu	1.006	1.351	1.03	0.776	1.472	0.414	1.01	1.00	0.98
Gd	4.724	6.27	4.822	2.024	3.891	1.047	3.80	4.00	3.50
Tb	0.72	0.881	0.721	0.349	0.658	0.192	0.59	0.70	0.75
Dy	3.64	4.71	3.777	2.223	3.308	1.194	3.14	5.00	2.60
Ho	0.702	0.918	0.766	0.439	0.604	0.256	0.61	0.60	0.78
Er	1.943	2.659	2.147	1.344	1.858	0.777	1.79	2.00	1.91
Tm	0.299	0.425	0.334	0.204	0.306	0.123	0.28	0.60	0.66
Yb	1.875	2.655	2.019	1.321	2.214	0.832	1.82	3.00	2.80
Lu	0.297	0.427	0.323	0.238	0.41	0.158	0.31	0.40	0.46
∑REE	224.20	341.92	209.79	148.64	220.23	73.06	202.98	153.8	182.95
∑LREE/∑HREE	14.79	17.05	13.07	17.26	15.62	14.95	15.45	8.44	–
Eu/Eu*[e]	0.72	0.69	0.70	0.89	0.93	0.96	0.77	0.83	0.80
Ce/Ce*[e]	1.77	1.92	1.53	0.98	0.89	0.95	1.39	0.67	1.14
$(La/Yb)_n$	10.85	11.34	10.43	14.06	12.23	11.24	11.59	7.56	7.69
$(La/Sm)_n$	4.47	4.89	4.78	5.03	4.22	5.30	4.69	6.22	5.02
$(Gd/Yb)_n$	1.34	1.25	1.27	0.81	0.93	0.67	1.11	0.71	0.66

[>] Represents out of the limit of the ICP-MS machine. –Represents no data

Average value of seven analyzing results with deviation in percentage less than 10%

[a] Average concentration of soil samples from S1 to S6

[b] World soils values suggested by Bowen (1979)

[c] Regional soils of Hunan province after Li and Zhen (1988)

[d] EI represents the enrichment index calculated by the equation seen in the text

[e] $Eu/Eu^{*} = (Eu)_n/((Sm)^{*}_n(Gd)_n)^{1/2}$, $Ce/Ce^{*} = (Ce)_n/((La)^{*}_n(Pr)_n)^{1/2}$

upper continent crust (Taylor and Mclennan 1995) and plotted in order of increasing ionic radius in Fig. 5. A tendency of increasing depletion towards the smaller cations is clearly shown. This is similar to the pattern Nesbitt et al. (1980) observed for weathering profiles and suggests that the waste rocks are weathered to a moderate degree. Relative to other smaller cations, depletion of Sr is particularly severe, also implying that the weathering of waste rocks is dominated by decomposition of K-feldspar.

The REE patterns (Fig. 6a) of waste rocks are uniform and similar to the average black shale (Mason and Morre 1982), with LREE enrichment (high $(La/Yb)_n$, $(La/Sm)_n$ and LREE/HREE ratios), flat HREE [$(Gd)_n/(Yb)_n$=0.91–1.26, average 1.09] and significant negative Eu-anomalies (Eu/Eu^{*} average of 0.76) and

Table 6 Concentrations (ug/l) of heavy metals, trace elements, major elements and rare earth elements in water from Taohuajiang watershed

Sample	W1	W2	W3	SW[b]	W4	W5	TW[b]	RGW[b]
pH	6.5	6.5	6.8		6.5	6.8		
Major elements								
Al	28.62	95.81	438.7	187.71	11.8	5.39	8.595	241.104
Ti	2.167	2.147	5.746	3.35	1.16	1.155	1.158	–
Fe	753.10	683.80	941.60	792.83	162.20	185.30	173.75	–
Na	15,358.9	13,468.6	12,805.1	13,877.53	3,052.10	3,004.8	3,028.45	29.473
K	3,769.20	12,879.7	11,610	9,419.63	1,987.50	1,843.6	1,915.55	4.53
Ca	148,609.1	121,192.7	114,256.3	128,019.4	39,370.6	38,839.1	39,104.85	21.584
Mg	64,273.9	39,962	36,743.4	46,993.1	5,853.4	6,225.4	6,039.4	1.942
Ba	50.43	76.44	66.35	64.407	145.80	147.20	146.50	85.47
Rb	6.541	37.28	31.44	25.087	1.149	0.826	0.988	0.019
Sr	2,539.40	2,044.9	1,897.4	2,160.57	145.80	144.7	145.25	0.002
Cs	12.80	12.29	11.35	12.1467	0.027	0.018	0.0225	–
P	29.06	13.87	49.62	30.85	17.23	17.43	17.33	1.19
Heavy metals								
As	0.11	0.032	0.092	0.078	0.008	0.008	0.008	0.109
Mo	10.08	13.59	11.11	11.593	1.179	1.419	1.299	0.181
U	4.214	2.013	4.925	3.717	0.27	0.225	0.248	0.11
Sb	0.022	0.023	0.02	0.0217	0.01	0.01	0.01	0.027
Se	–	–	–	–	–	–	–	0.293
Cd	0.062	0.06	0.068	0.063	0.015	0.008	0.012	1.407
Co	0.354	1.606	3.833	1.931	0.102	0.198	0.15	2.942
Cr	14.10	11.50	10.26	11.953	14.80	15.03	14.915	6.887
Cu	0.959	0.922	4.418	2.10	0.668	0.53	0.599	1.397
Zn	9.708	15.76	15.66	13.709	14.84	13.75	14.295	18.858
Pb	0.957	1.342	7.079	3.126	0.899	0.901	0.90	6.316
Mn	9.392	1,443.2	1,779.80	1,077.46	2.531	0.298	1.415	0.001
Ni	24.24	40.45	50.09	38.26	0.575	0.743	0.659	–
Sc	3.089	3.368	3.506	3.321	2.012	2.149	2.08	–
Sn	0.021	0.009	0.014	0.0147	0.014	0.011	0.0125	0.001
Tl	0.296	0.315	0.34	0.317	0.037	0.025	0.031	1.347
Th	0.003	0.003	0.10	0.035	0.002	0.001	0.0015	–
V	2.492	2.567	2.938	2.666	3.018	2.82	2.919	–
Other trace elements								
Bi	0.002	0.001	0.01	0.0043	0.003	0.001	0.002	–
Nb	0.029	0.004	0.005	0.013	0.007	0.033	0.02	–
Ta	–	0.001	0.001	0.0007	–	–	–	0.001
Zr	0.041	0.055	0.093	0.063	0.008	0.007	0.0075	–
Hf	–	0.001	0.004	0.0017	–	–	–	–
Y	0.041	0.242	0.612	0.298	0.016	0.006	0.011	–
Ga	0.514	0.738	0.653	0.635	1.495	1.597	1.546	–
Ge	0.047	0.032	0.039	0.0393	0.015	0.02	0.0175	–

Sample	W6	W7	W8	W9	W10	W11	W12	RW[a]	W13	W14	FW[a]
pH	6.8	6.5	7.0	6.8	6.8	7.0	7.0		6.0	6.2	
Major elements											
Al	32.71	33.02	20.64	29.9	36.54	137.3	30.8	45.844	36.65	14.85	25.75
Ti	2.17	1.365	1.047	1.256	0.557	1.437	1.749	1.369	2.479	2.392	2.4355
Fe	47.38	29.22	19.34	66.2	22	33.91	24.92	34.71	77.83	70.42	74.125
Na	2,053.5	1,438.6	1,282.4	1,322.7	1,680.1	541.7	3,146	1,637.857	4,236.4	4,273.6	4,255
K	703.2	611.7	387	520.4	1203.8	496.5	1180	728.943	732.2	726.3	729.25
Ca	2,081	4,450.3	2,165	2,891.9	17,507.2	3,619.8	3,170.3	5,126.5	4,665.4	4,748.3	4,706.85
Mg	3,351.5	1,847	1,503.1	1,960.2	3,258.9	1,279.1	1,556.2	2,108	2,275.2	2,254	2,264.6
Ba	0.346	72.25	12.26	8.48	67.33	86.65	35.02	40.334	20.82	21.15	20.985
Rb	4.161	0.556	1.352	2.78	1.457	0.834	2.238	1.911	0.385	0.38	0.3825
Sr	9.769	15.94	14.77	13.31	77.32	13.48	21.44	23.718	28.33	28.44	28.385
Cs	1.277	0.024	0.685	0.896	0.037	0.036	0.013	0.424	0.005	0.003	0.004
P	29.46	34.45	7.211	41.48	12.92	6.656	13.68	20.837	32.68	41.31	36.995

Table 6 continued

Sample	W6	W7	W8	W9	W10	W11	W12	RW[a]	W13	W14	FW[a]
pH	6.8	6.5	7.0	6.8	6.8	7.0	7.0		6.0	6.2	
Heavy metals											
As	0.194	0.013	0.091	0.189	0.048	0.005	0.006	0.078	0.002	0.003	0.0025
Mo	1.636	0.081	0.014	0.037	0.77	0.088	0.01	0.377	0.083	0.073	0.078
U	0.01	0.01	0.01	0.01	0.3	0.085	0.01	0.062	0.005	0.004	0.0045
Sb	0.01	0.01	0.01	0.01	0.01	0.01	0.01	0.01	0.001	0.001	0.001
Se	0.122	0.129	0.118	0.1	0.204	0.248	0.107	0.147	–	–	
Cd	0.026	0.021	0.09	0.022	3.407	0.104	0.036	0.529	0.007	0.007	0.007
Co	0.056	0.022	0.036	0.024	0.057	0.408	0.025	0.0897	0.043	0.043	0.043
Cr	8.446	2.739	3.952	4.561	7.054	3.865	7.936	5.508	4.318	4.171	4.2445
Cu	1.182	0.427	0.653	0.23	6.069	1.112	0.109	1.397	0.354	0.395	0.3745
Zn	10.43	2.784	11.44	3.457	17.07	2.601	2.619	7.200	9.7	9.144	9.422
Pb	0.051	0.07	0.088	0.041	0.078	0.106	0.061	0.071	1.197	0.946	1.0715
Mn	2.249	0.342	3.097	7.385	2.149	14.58	5.065	4.981	0.543	0.451	0.497
Ni	2.817	0.372	2.739	0.97	4.172	1.069	0.784	1.846	0.797	0.779	0.788
Sc	2.523	1.477	1.202	1.425	0.858	1.159	2.169	1.545	3.341	3.361	3.351
Sn	0.01	0.01	0.01	0.01	0.01	0.01	0.01	0.01	0.008	0.006	0.007
Tl	0.02	0.026	0.033	0.021	0.071	0.061	0.019	0.0359	0.014	0.018	0.016
Th	0.01	0.01	0.01	0.01	0.01	0.01	0.01	0.01	0.009	0.007	0.008
V	0.156	0.401	0.126	0.16	2.161	0.653	0.158	0.545	2.303	2.071	2.187
Other trace elements											
Bi	0.035	0.01	0.01	0.01	0.01	0.01	0.01	0.0136	0.003	0.003	0.003
Nb	0.01	0.01	0.01	0.01	0.01	0.01	0.01	0.01	0.002	0.002	0.002
Ta	0.004	0.003	0.003	0.002	0.003	0.003	0.003	0.003	–	–	
Zr	0.024	0.042	0.027	0.017	0.009	0.071	0.015	0.0293	0.045	0.021	0.033
Hf	0.001	0.002	0.001	0.001	0.001	0.002	0.001	0.0013	–	–	
Y	0.006	0.015	0.011	0.006	0.035	0.432	0.055	0.08	0.019	0.018	0.0185
Ga	0.019	1.86	0.335	0.234	1.842	2.382	0.982	1.093	0.234	0.227	0.2305
Ge	0.028	0.023	0.029	0.035	0.025	0.026	0.023	0.027	0.015	0.022	0.0185

–Represents no data

[a] Average value of seven analyzing results with deviation in percentage less than 10%

[b] SW, TW, RGW, RW and FW represent average values of stream waters, tap waters, regional waters (after Zhang et al. 1996), reservoir waters and fountain waters, respectively

slightly negative Ce-anomalies (Ce/Ce^{*} =0.85–1.00, average 0.94), except M-1. There are no systematic differences between REE patterns of MWR and BWR, but the significant Ce-anomalies and high content of total REE of MWR show that the MWR was formed under oxygen conditions, or it has oxidized more extensively than BWR since being exposed.

The contents of heavy metals (V, Mn, Ni, Cu, Zn, Pb, Mo, Cd and Sb) in the waste rocks are distinctly variable, but others (Sc, Cr, Th, U, Sn and Tl) are relatively constant in the BWR (Table 4). The MWR contains much higher contents of Co, Ni, Cu, Pb and Mo (193.70, 1069.0, 317.20, 137.90 and 77.15 ppm, respectively) than the BWR (corresponding average of 38.96, 117.87, 100.26, 52.05 and 11. 29 ppm, respectively), indicating the high abundance of sulfide minerals such as millerite (NiS) and galena (PbS) in MWR, as observed under the microscope. Among these heavy metals, Sc, Cr and Th show clearly the positive corrections with K_2O (Fig. 4), implying the mobility of metals Sc, Cr and Th was dominated by the K-bearing minerals. Other metals, such as Co, Ni, Cu, Zn, Pb, Mo, Cd and Tl, are scattered with respect to K_2O, showing that these metals were controlled by other minerals, probably the sulfides. However, the above metals do not show corrections between each other (plots omitted), except the positive correction between Ni and Co (Fig. 4), indicating that the metal mobility was influenced by weathering, which might cause the decomposition of sulfides such as galena and pyrite, as observed under the microscope. A spidery diagram for all metals of waste rocks is shown in Fig. 7a; it is clear that the distribution patterns of the metals among the waste rocks are similar, implying the waste rocks (except M-1) were weathered to a similar degree. Also, the metal distributional patterns of both MWR and BWR are similar to the bedrock (T-2 and T-3), indicating clearly the genetic relation of both MWR and BWR to the bedrock.

Surrounding soils

The concentrations of heavy metals and REE of the surrounding soil samples are listed in Table 5. It is clear that the soils surrounding the waste rocks are enriched with the metals V, Cr, Co, Cu, Zn, Mo, Cd, Pb, Tl, Th and U, and depleted in As Se, and Hg, relative to both the world soils (Bowen 1979) and regional soils of Hunan province (Li and Zhen 1988). The enrichments of Cr, Cu, Zn, Mo, Cd, Pb, Tl, Th and U of the soils are 2.6, 6.5, 2.9, 8.3, 1.5, 4.2, 13.2, 1.9 and 2.1-fold, respectively, relative to the world soil (Bowen 1979), whereas the metals V, Mn and Co are variable among the soil samples, with the average higher than of the world soils (Bowen 1979).

Imitating the enrichment index (EI) suggested by Chon (1996), we calculate the EI of the soils by ratios of 11 heavy metal concentrations to corresponding values of the world soils (EI_{WS}; Bowen 1979) and regional soils of Hunan province (EI_{XS}; Li and Zhen 1988) using the following equations:

$$EI_{WS} = (V/90 + Cr/70 + Co/8 + Cu/30 + Zn/90 + Mo/1.2 + Cd/0.35 + Tl/0.2 + Pb/35 + Th/9 + U/2)/11 \quad (6)$$

$$EI_{XS} = (V/136 + Cr/67 + Co/15 + Cu/27 + Zn/95 + Mo/1.2 + Cd/0.093 + Tl/0.2 + Pb/27 + Th/16 + U/4.2)/11 \quad (7)$$

The calculated results listed in Table 5 show that both the EI_{WS} and EI_{XS} of the surrounding soils range from 2.07 to 8.26 and are all higher than 1.0, indicating that the soils are contaminated with the above heavy metals.

The spidery distribution patterns for metals in the soils (Fig. 7b) are similar to that of the waste rocks and bedrock, implying a genetic relation between the heavy metal contaminations of the soils and waste rock and bedrock weathering.

The concentrations of total REE for the soils range from 73 to 341 ppm, with an average of 202 ppm. This is more variable than the waste rock (204–305 ppm, average of 225 ppm). Moreover, the ΣLREE/ΣHREE ratios for the soils (=13–17, average 15.46) are distinctly higher than of waste rocks (=8.6–11.9, average 9.9), indicating the LREE might be enriched during the soil development processes, as Nesbitt (1979) concluded. The soil samples, S1, S2 and S3 have positive Ce-anomalies (Ce/Ce^* =0.89–1.92, average 1.35), which are similar to that of the MWR, suggesting an oxygenic condition for the soil development.

The REE distribution patterns of the soils (Fig. 6b) are also uniform, with LREE enrichment (higher $(La/Yb)_n$, $(La/Sm)_n$ and LREE/HREE ratios), flat HREE [$(Gd/Yb)_n$ =0.67–1.34, average 1.05] and significant negative Eu anormalies (Eu/Eu^* =0.70–0.96, average 0.81). These are significantly similar to the waste rocks and bedrock, also implying a genetic relation of the soil development to weathering of the waste rock and bedrock.

Surface water

The concentrations of major elements, heavy metals and other trace elements as well as pH values of all water samples are listed in Table 6. Generally, the waters from the stream, the reservoir and the tap-water system pumped from the reservoir are meteoric in origin, whereas the fountain waters have a different origin. Table 6 shows that the concentrations of major alkalis and alkaline earths (Ca, Mg, Na, K and Sr) and major elements (Fe, P) are distinctly higher in the meteoric waters than the fountain waters. It is clear that the contents of these elements decrease gradually from the stream water to tap water, then to reservoir waters. For example, the average concentration of iron decreases from 792.83 to 173.75 (μg/l), and then to 34.71 (μg/l), respectively (Table 6). Moreover, the spidery diagram of major elements of all water samples (Fig. 7e) shows similar distribution patterns to meteoric waters, implying the meteoric waters are similar in chemical composition.

The highest concentrations of Rb, Sr and Cs coincide with maximum contents of Na, Mg and Ca, suggesting enhanced leaching in response to greater dissolution of carbonates. The concentrations of major alkalis and alkaline earths significantly decrease from the headwaters (stream waters) to middle-river (tap waters), to downriver (reservoir waters), suggesting the meteoric waters were gradually diluted along its pathway.

The major alkalis and alkaline earths (Ca, Mg, Ba, Cs and P) are extremely enriched in the meteoric water samples compared to the regional surface waters (Zhang et al. 1996). For example, the enrichment factors (EF) of Ca from the stream waters, tap waters and reservoir waters gradually decrease from 4,343.6 to 1,326.8, and to 173.9, respectively. The concentrations and distribution patterns of major alkalis and alkaline elements (Ca, Mg, Na, K and Sr) and major elements (Fe and P) in the meteoric waters indicate that the headwaters are more greatly impacted by leaching of chemical components from waste rocks and bedrock weathering.

The concentrations of heavy metals in water samples show similar features to the above major alkalis and alkaline elements. In particular, (1) the concentrations of heavy metals in the meteoric waters are distinctly higher than the fountain waters (Table 6); (2) the concentrations of most heavy metals (Cd, Co, Cr, Cu, Pb, Mn, Ni and V) gradually decrease from of the stream waters to tap waters, and then to reservoir waters (Table 6); (3) most heavy metals show similar spidery distribution patterns (Fig. 7c, d), on which the heavy metals (V, Cr, Co, Cu, Zn, Mo, Cd, Hg, Tl, Pb, Th and U) of the stream waters and tap waters (Fig. 7c) are slightly different from that of the reservoir waters (Fig. 7d), but similar to both the soils and waste rocks (Fig. 7a, b); (4) compared to the regional surface water (Zhang et al. 1996), the meteoric waters are enriched with many heavy metals (Table 6). The stream waters are enriched with Cd, Co, Zn, Pb, Mn, Ni, Sc, Th and V, whereas the tap waters and reservoir waters are enriched only in Cr, Zn, Sc, Th and V, indicating dilution from the stream waters to the reservoir water.

The mineralogical study shows that the element S was lost during weathering, but the pH conditions of surface waters do not show a development of acid drainage formed during weathering. This is possibly due to the oxidation of carbonates, which consumed the acidity released by sulfide mineral oxidation, as suggested by Blowes et al. (1998). The pH values of stream waters range from 6.5 to 6.8, and those of the reservoir and pipe waters are from 6.8 to 7, consistent with dilution suggested by concentrations of major alkalis and alkaline earths and heavy metals. Therefore, the neutralization might be the cause for the dilution of major alkalis and alkaline earths and heavy metals through chemical precipitating.

Discussion

The mineralogical study shows that the waste rocks at the Xiaotaoyuan mine are currently undergoing chemical weathering. The Mn carbonates and the sulfide minerals such as pyrite, galena and chalcopyrite are being oxidized, and S and the metals Co, Cu, Ni, Au and Ag are being released during sulfide decomposition. The geochemical characteristics of major elements of the waste rock imply that oxidation of Mn carbonate and sulfide minerals is accompanied by decomposition of K-feldspar (Rao and Fan 1990; Zhu 1996; Wu and Cao 2003). The rare earths Rb, Sr and Cs are released due to decomposition of Mn carbonates, and Cr, Sc and Th are dispersed owing to the breaking of K-feldspar.

It is difficult to answer whether the carbonates hosted within the waste rocks acted as barriers for metal mobility (Lapakko et al. 1997; Holmstrom et al. 1999) or promoted sulfide oxidation (Evangelou and Huang 1994; Dold and Fontbote 2002) during weathering. However, the mineralogical observations suggest that sulfide oxidizing is actually taking place along with the carbonate oxidation during weathering, as observed by Blowes et al. (1998).

The pH values of the surface waters suggested that carbonate oxidation neutralizes acid drainage caused by sulfide oxidation during weathering, through releasing CO_2 by chemical reactions (1), (2) and (3). Moreover, the geochemical studies show that the heavy metals Cr, Cu, Zn, Mo, Cd, Pb, Tl, Th and U are enriched in the surrounding soils, and Cd, Co, Cr, Cu, Pb, Mn, Ni and V in the surface water system. Therefore, it is suggested that carbonate hosted within the waste rocks does not inhibit sulfide oxidation and metal mobility.

The heavy metals in both surrounding soils and surface waters were probably leached from waste rock and/or bedrock during mineral (mostly sulfide, carbonate and K-feldspar) decomposition. The evidence for this comes from: (1) mineralogical observations under the microscope and EMPA and EDS analyzing results (Tables 2, 3); (2) similar REE distribution patterns among waste rocks, bedrock and surrounding soils (Fig. 6); (3) similar spidery distribution patterns for the metals V, Cr, Co, Cu, Zn, Mo, Cd, Hg, Tl, Pb, Th and U in the waste rocks and bedrock, and the surrounding soils, and the surface waters (Fig. 7a–d). The enrichment indices (EI_{WS} and EI_{XS}; Table 5) of the surrounding soils suggest that the soils may be contaminated with a number of heavy metals. The heavy metal contamination in the surrounding soils and surface water is probably caused by the release of heavy metals from sulfide decomposition during waste rock and bedrock weathering.

There are two usual mechanisms for the mobility of heavy metals during weathering: release (loss) and secondary enrichment (gain). A mass-balance calculation is generally applied to estimate metal mobility during weathering (e.g., Nestbitt 1979; Middelburg et al. 1988; Kurtz et al. 2000; Peng et al. 2004). The percentage of loss (% loss) can be calculated relative to an immobile index element, assuming that the total inventory of the index element on each weathering waste rock does not change through time and that the index element has not been redistributed among the waste rocks. The fraction of mass lost from waste rock relative to the mass, j, originally present (represented by fresh bedrock T-2) is calculated from the following

equation (Nestbitt 1979; Middelburg et al. 1988; Nesbitt and Wilson 1992; Kurtz et al. 2000):

$$\%\ \text{loss} = (C_{j,w}/C_{j,p} \times C_{i,p}/C_{i,w} - 1) \times 100 \quad (8)$$

where C represents the concentration of any element in any of the analyzed samples, the subject j refers to the selected element for calculation, the subscript i refers to the immobile element selected for calculation and the subscripts w and p refers to waste rock and parent material (bedrock T-2 in this study), respectively.

Most important for the calculations is to determine the immobile index element. In recent years, Nb, Ta, Ir and Zr have been commonly considered as immobile index elements for the calculation because of their low aqueous solubility (Kurtz et al. 2000; Jaffe et al. 2002; Peng et al. 2004). The present data show that the element Zr is in variable concentrations in different waste rocks, but ratios of Zr/Hf, Zr/Nb and Zr/Ta are relatively constant among the waste rocks and bedrock (Table 4; Fig. 4). This implies that Zr remains immobile during weathering. Therefore, we consider Zr as an immobile index element in these discussions of heavy metal loss during exposure weathering. The calculation results are shown in Fig. 8.

It is clear that (1) for MWR sample (M-1), some metals (Sc, V, Cr, Th, U, Sn and Cd) were released, but others (Co, Ni, Cu, Zn, Pb, Mo, Sb and Tl) were probably enriched during weathering, (2) for BWR samples, most heavy metals (Sc, V, Cr, Th, U, Sn, Co, Ni, Cu, Zn, Pb, Mo, Cd, Sb and Tl) were lost during weathering, and (3) the metals V and Cd were strongly released from all the waste rocks during exposure weathering.

The above evidence for metal mobility during weathering suggests that most heavy metals (Sc, V, Cr, Th, U, Sn, Co, Ni, Cu, Zn, Pb, Mo, Cd, Sb and Tl) are released from the waste rocks, even though some are enriched in samples M-1 and M-6, which have a high concentration of CaO (Table 4). However, no evidence for the secondary enrichment was observed under the microscope. Therefore, we conclude that the waste rocks at Xiangtaoyuan mine are a source for heavy metal contamination to the environment, that is, the surrounding soils and surface water.

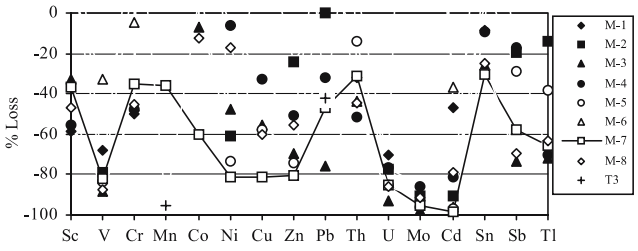

Fig. 8 Diagram of % loss of heavy metals from waste rocks (for details, see the text)

A comparison of the metals released from waste rocks and bedrock (Fig. 8) to those enriched in both surrounding soils and surface waters (Tables 5, 6; Fig. 7b, c) reveals a mirror-image relationship between them. The metals released from waste rocks and bedrock are the source of heavy metal contamination in the surrounding environment (soils and surface waters).

Conclusions

This preliminary study on mineralogy and geochemistry of the waste rocks piled at Xiangtaoyuan in the Taojiang Mn-ore district resulted in the following:

(1) The waste rocks are currently undergoing chemical weathering and characterized by decomposition of the Mn carbonates (mainly kutnohorite and rhodochrosite), K-feldspar and the sulfide minerals such as galena, pyrite and chalcopyrite.

(2) The decomposition of the Mn-carbontaes, K-feldspar and sulfide minerals during waste rock weathering may cause the emission of major alkalis and alkaline elements (Ca, Mg, Na, K, Rb, Sr and Cs), major elements (Fe, S and P) and heavy metals (V, Co, Ni, Cu, Zn, Pb, Mo, Cd, Sb and Tl). The release of major alkalis and alkaline elements is mainly controlled by decomposition of Mn-carbonates. The dispersion of Cr, Sc and Th is related to weathering of K-feldspar, and the emission of major elements and heavy metals is dominantly due to breaking of sulfide minerals such as pyrite, galena and chalcopyrite.

(3) The oxidation of Mn-carbonates was accompanied by oxidation of sulfide minerals, during which the Mn carbonate does not act as a barrier to metal mobility.

(4) The metals released from waste rock and bedrock weathering (including Sc, V, Cr, Th, U, Sn, Co, Ni, Cu, Zn, Pb, Mo, Cd, Sb and Tl) are dispersed directly to environments and accumulate in the surrounding soils and surface water system.

(5) The waste rocks distributed throughout the mining area are an important source of heavy metal contamination in the area. This may cause very serious environmental and health problems for the local people, and necessary measures should be taken to treat the waste rocks to protect the local environment.

Acknowledgments This study was supported by the National Scientific Foundation Committee of China grant number 40572172 and 40002021. We are grateful to MSc Latkiewicz at the Institute of Geological Science, Jagiellonian University (Poland), for help the EDS study. Mr. Xianglin Tu at the Guangzhou Institute of Geochemistry (CAS) is thanked for help for the ICP-MS/AES analyses. The authors wish to thank Dr. G. Beardsmore at Monash University, Australia, for improving the English language of the manuscript and Dr. T. F. Zhou for an official review.

References

Akpan ER, Ekpe UJ, Ibok UJ (2002) Heavy metal trends in the Calabar River, Nigeria. Environ Geol 42:47–51

Audry S, Blance G, Schafer J (2005) The impact of sulphide oxidation on dissolved metal (Cd, Zn, Cu, Cr, Co, Ni, U) inputs into the Lot-Garonne fluvial system (France). Appl Geochem 20:919–931

Bhatia MR (1983) Plate tectonics and geochemistry composition of sandstones. J Geol 91:611–627

Blowes DW, Jambor JL, Hanton-Fong CJ (1998) Geochemical, mineralogical and microbiological characetristion of a sulphide-bearing carbonate-rich gold-mine tailings impoundment, Joutel, Quebec. Appl Geochem 13(6):687–705

Boulet M, Larcoque ACL (1998) A comparative mineralogical and geochemical study of sulfide mine tailings at sites in New Mexico, USA. Environ Geol 33:130–142

Bowen HJM (1979) Plants and chemical elements. Academic, London

Chon HT, Cho CH, Kim KW, Moon HS (1996) The occurrence and dispersion of potentially toxic elements in areas covered with black shales and slates in Korea. Appl Geochem 11:69–76

Coveney RM Jr, Grauch RI, Murowchick JB (1994) Metals, phosphate and stone coal in the Proterozoic and Cambrian of China. SEG Newsl 18:1–11

Dold B, Fontbote L (2002) A mineralogical and geochemical study of element mobility in sulfide mine tailings of Fe oxide Cu–Au deposits from the Punta del Cobre belt, north Chile. Chem Geol 189:135–163

Emsbo P, Hofstra AH, Johnson CA, Koenig A, Grauch R, Zhang XC, Hu RZ, Su WC, Pi DH (2005) Lower Cambrian metallogenesis of south China: interplay between diverse basinal hydrothermal fluids and marine chemistry. In: Mao JW, Bierlein FP (eds) Mineral research: meeting the global challenge, vol 1. Springer, Berlin Heidelberg New York. pp 115–118

Evangelou VP, Huang X (1994) Infrared spectroscopy evidence of an iron carbonate complex on the surface of pyrite. Spectrochim Acta 50(A):1333

Fan DL, Zhang T, Ye J (2004) The black shales distributed in China and their relative ore deposits. Science Press, Beijing, pp 260–343 (in Chinese)

Fanani L, Zuddas P, Chessa A (1997) Heavy metals speciation analysis as a tool for studying mine tailings weathering. J Geochem Explor 58:241–248

Feng R, Kerrich R (1990) Geochemistry of fine-grained clastic sediments in the Archean Abitibi greenstone belt, Canada: implications for provenance and tectonic setting. Geochim et Cosmochim Acta 54:1061–1081

Frostner U, Wittman GTW (1981) Metal pollution in the aquatic environment, 2nd edn. Springer, Berlin Heidelberg New York

Fu QH (2001) The geological and geochemical characteristics of Taojiangtype manganese deposits. Hunan Geol 20(1):15–20

Holmstrom H, Ljungberg J, Ohlander B (1999) Role of carbonates in mitigation of metal release from mining waste, evidence from humidity cells tests. Environ Geol 37(4):267–280

Jaffe LA, Peucker-Ehrenbrink B, Petsch ST (2002) Mobility of rhenium, platinum group elements and organic carbon during black shale weathering. Earth Planet Sci Lett 198:339–353

Jiang DH, Yang ZQ, Zhao SJ (1995) Studies of ore-forming process of ''Taojiang type manganese'' of the middle Ordovician in central Hunan province. Acta Sedimentologica Sinica 13(1):59–67 (in Chinese with English abstract)

Jung BH, Yun ST, Mayer B, Kim SO, Park SS, Lee PK (2005) Transport and sediment-water partitioning of trace metals in acid mine drainage: an example from the abandoned Kuangyang Au-Ag mine area, South Korea. Environ Geol 48:437–449

Kuang OG, Zhao YH, Wu YS, Li YL (2003) Effects of structural controlling on spatial distribution of the ''Taojiang style'' manganese deposits. Geol Prospect 39(1):32–35 (in Chinese with English abstract)

Kurtz AC, Derry LA, Chadwick OA, Alfano MJ (2000) Refractory element mobility in volcanic soils. Geology 28:683–686

Lakhan VC, Cabana K, LaValle PD (2002) Heavy metal concentrations in superficial sediments from accreting and eroding areas along the coast of Guyana. Environ Geol 42:73–80

Lapakko K, Antonson DA, Wanger JR (1997) Mixing of limestone with finely-crushed acid producing rock. ICARD, Vancouver, pp 1345–1360

Larocque AC, Rasmussen PE (1998) An overview of trace metals in the environment, from mobilization to remediation. Environ Geol 33(2/3):85–90

Lavergren U (2005) Black shales as a metal contamination source. ESS Bull 3(1):18–31 (from website: http://www.bom.hik.se/ess)

Li J, Zheng CJ (1988) Handbook for background values of elements in environments. China Environmental Science Press, China, pp 123–238 (in Chinese)

Lu L, Wang RC, Chen FR, Xue JY, Zhang PH, Lu JJ (2005) Element mobility during pyrite weathering: implications for acid and heavy metal pollution at mining-impacted sites. Environ Geol 49:82–89

Malmstrom ME, Gleisner M, Herbert RB (2006) Element discharge from pyretic mine tails at limited oxygen availability in column experiments. Appl Geochem 21:184–202

Mason B, Morre CB (1982) Principles of geochemistry, 4th edn. Wiley, New York, pp 46, 47, 176–177

McLennan SM, Taylor SR, McCulloch MT, Maynard JB (1983) Geochemistry of Archean shales from the Pilbarab Supergroup, western Australia. Geochim Cosmochim Acta 47:1211–1222

Middelburg JJ, Weijden CV, Woittiez JRW (1988) Chemical processes affecting the mobility of major, minor and trace elements during weathering of granitic rocks. Chem Geol 68:253–273

Moncur MC, Ptacek CJ, Blowes DW, Jambor JL (2005) Release, transport and attenuation of metals from an old tailings impoundment. Appl Geochem 20:639–659

Neaman A, Flore M, Trolard F, Borrie G (2004) Improved methods for selective dissolution of Mn oxides: applications for studying trace element associations. Appl Geochem 19:973–979

Nesbitt HW, Muir IJ (1994) X-ray photoelectron spectroscopic study of pristine pyrite surface reacted with water vapour and air. Geochim Coschim Acta 58:4667–4679

Nesbitt HW, Wilson RE (1992) Recent chemical weathering of basalts. J Sci 292:740–777

Nesbitt HW, Markovics G, Price RC (1980) Chemical processes affecting alkalis and alkaline earths during continent weathering. Geochim Cosmochim Acta 44:1659–1666

Nestbitt WH (1979) Mobility and fractionation of rare earth elements during weathering of a granodiorite. Nature 279:206–210

Nurnberg HW (1984) The voltammertric approach in trace metal chemistry of natural waters and atmospgeric precipitation. Anal Chem Acta 164:1–21

Pasava J, Kribek B, Zak K, Li C, Deng HL, Zeng M (2003) Preliminary results of the study of toxic elements in soils and crop plants in areas of Ni–Mo black shale-hosted deposits (Zunyi region, south China). In: Eliopoulos et al. (eds) Mineral exploration and substantial development, Millpress, Rotterdam, pp 53–56

Peng B, Song ZL, Tu XL, Lv HZ, Wu FC (2004) Release of heavy metals during weathering of the Lower Cambrian black shales in western Hunan, China. Environ Geol 45(8):1137–1147

Peng B, Wu FC, Xiao ML, Xie SR, Lu HZ, Dai YN (2005) The resource functions and environment effects of black shales. Bull Mineral Petrol Geochem 24(2):153–158 (in Chinese with English abstract)

Petsch ST, Berner RA, Eglinton TI (2000) A field study of the chemical weathering of ancient organic matter. Org Geochem 31:475–487

Peucker-Ehrenbrink B, Hannigan R (2000) Effects of black shale weathering on mobility of rhenium and platinum group elements. Geology 28:475–478

Rao XF, Fan DL (1990) Petrology and geochemistry of black shales of the middle Ordovician in Taojiang, central Hunan. Acta Petrol Sinica 3:78–86 (in Chinese with English abstract)

Silva EF, Zhang CS, Pinto LS, Patinha C, Reis P (2004) Hazard assessment on arsenic and lead in soils of Castromil gold mining area, Portugal. Appl Geochem 19:887–898

Sun CS (1995) Exploitation for poor and thin manganese resource in the Taojiang manganese mine. Hunan Geol 14(3):187–189 (in Chinese with English abstract)

Talyor SR, Mclennan SM (1995) Geochemical evolution of the continent crust. Rev Geophys 33:241–265

Wu YS, Cao JL (2003) Geochemistry traits of high grade Mn-ores of the middle Ordocician epoch in central Hunan. Hunan Geol 22(2):101–106 (in Chinese with English abstract)

Zhang LC, Yu ZS, Zhang S (1996) Chemical elements in aquatic environments. China Environmental Press, China, pp 190–194

Zhu SQ (1996) Characteristics of Taojiang-type hydrothermal sedimentary manganese deposits. Geol Rev 42(5):397–404 (in Chinese with English abstract)

Zhu KJ, Yao GL, Huang JH (1998) The geochemical process of Mn ore-capping in Taojiang manganese deposit. Geol Explor 13(3):1–8 (in Chinese with English abstract)